

Internalization of Auger electron-emitting isotopes into cancer cells: A method for spatial distribution determination of equivalent source terms

G. Royle, N. Falzone, R. Chakalova, K. Vallis & S. Myhra

To cite this article: G. Royle, N. Falzone, R. Chakalova, K. Vallis & S. Myhra (2016): Internalization of Auger electron-emitting isotopes into cancer cells: A method for spatial distribution determination of equivalent source terms, International Journal of Radiation Biology

To link to this article: <http://dx.doi.org/10.1080/09553002.2016.1233369>



View supplementary material [↗](#)



Accepted author version posted online: 07 Sep 2016.
Published online: 07 Sep 2016.



Submit your article to this journal [↗](#)



View related articles [↗](#)



View Crossmark data [↗](#)

Internalization of Auger electron-emitting isotopes into cancer cells: A method for spatial distribution determination of equivalent source terms

G. ROYLE¹, N. FALZONE^{1,3*}, R. CHAKALOVA², K. VALLIS¹ and S. MYHRA^{2*}

¹CRUK/MRC Oxford Institute for Radiation Oncology, Department of Oncology, University of Oxford, Oxford, United Kingdom

²Department of Materials, Begbroke Science Park, University of Oxford, Oxford, United Kingdom

³Department of Biomedical Science, Tshwane University of Technology, Pretoria, South Africa

*Corresponding authors

Dr. S. Myhra

Dr. N. Falzone

Email: *sverre.myhra@materials.ox.ac.uk*

Email: *nadia.falzone@oncology.ox.ac.uk*

Tel: +44 (0) 1865 225841

Tel: +44 (0) 1865 225841

Fax: +44 (0) 1865 857127

Fax: +44 (0) 1865 857127

Running title: Intracellular Auger electron emitter distribution

Keywords: Micro-dosimetry, photoresist, Auger electron-emitters, AFM, autoradiography

ABSTRACT

Purpose: A challenge for single cell dosimetry of internalised Auger electron-emitting (AE) radiopharmaceuticals remains how best to elucidate their spatial distribution. To this end, a method, photoresist autoradiography (PAR), was previously developed to identify the lateral spatial distribution of AE emitting radionuclides internalized in single cancer cells. In this report, we present a simple mathematical model based on the radius and depth of radiation-induced patterns in photoresist material to identify the location in the z-plane of an ^{111}In source capable of generating the pattern.

Material and Methods: SQ20B cells, derived from a head and neck squamous cell carcinoma, were exposed to ^{111}In -labeled epidermal growth factor (EGF) (8 MBq/ μg). The integrated electron fluence after 4 half-lives from the internalized radionuclide-containing construct was detected by a photoresist layer that was placed in close proximity to the cells. The resultant latent patterns were chemically developed and analysed by atomic force microscopy (AFM). The features in the patterns were matched to locations of electrons emitted from simulated point sources, thereby determining the likely locations of internalized radionuclides.

Results: The modeling procedure was validated using simple patterns. The model relates the depth and radius (in the x-y plane) of a pattern to the location and fluence of the source giving rise to the pattern. This point source modeling method provided a good fit to experimental data and can be expanded to analyze more complex patterns.

Conclusions: We have demonstrated the utility of the modelling technique to identify the location of internalized AE-emitting radionuclides. This methodology now needs to be extended to predict the source positions in more complex PAR patterns.

Introduction

Molecularly targeted radiotherapy is an important therapeutic tool in the treatment of a range of cancers (Jackson et al., 2013). Evaluation of a targeted radiotherapeutic at the preclinical stage of development begins with in vitro analysis of single cells. In the clinical setting treatment planning requires estimation of the total radionuclide dose and its distribution for each individual patient. The calculation of absorbed radiation dose from a radiotherapeutic is currently based on image acquisitions with spatial resolution of the radioactivity distribution in the mm-range (Howell et al., 2012, Malaroda et al., 2005). At present the clinical response to internal radionuclides is related to the macroscopic (i.e. whole-tumour or whole-organ) absorbed dose that is based implicitly on the assumption of uniform distributions of activity and energy deposition (Howell et al., 2012). The work described in this paper is a continuation of previous efforts motivated by the need to obtain more detailed sub-cellular information about the uptake and spatial distribution of Auger electron-emitting radiopharmaceuticals.

A novel electron autoradiography technique, photoresist autoradiography (PAR), was recently proposed and reported (Falzone et al., 2012, Falzone et al., 2011, Royle et al., 2015). It is based on a photoresist polymer as the detecting medium and atomic force microscopy (AFM) as the read-out device of a 3-D pattern in the resist. The PAR concept was originally concerned with mapping the locations of internalized radionuclides in the x-y plane, and with relating the volume of the pattern to the total number of electrons from all internalized sources reaching the resist surface (Royle et al., 2015). In comparison to the well-established micro-autoradiography (MAR) technique (Puncher and Blower, 1994), PAR carries the possibility of greater lateral spatial resolution and scope for quantitative interpretation. In this report a refinement of the analytical approach to patterns etched into photoresists by exposure to radionuclides is presented. It is shown that a simple model applied to an experimentally

obtained AFM pattern, allows the determination of the total fluence of the intracellular source terms that gave rise to that pattern and also describes the location of the sources in x-y-z space.

[Figure 1]

The schematic shown in Figure 1 is a flowchart of a typical experiment. Firstly cells are treated with an Auger electron-emitting radiotherapeutic, nuclei are isolated and the PMMA photoresist film coated onto a silicon substrate is inverted and placed in close proximity above the cells/nuclei located on a flat substrate. During a period of four half-lives, the decaying internalized radionuclides isotropically emit internal conversion and Auger electrons. A fraction of electrons enter the photoresist and, when the fluence is sufficient, produce spatially-resolved, latent images in the PMMA. After chemical development, the latent images are converted into a pattern of pits. The final step is the AFM topographical imaging of the 3-D structures in the resist.

Materials and Methods

Preparation of photoresist films and post-exposure processing

The resist film, NANOTMPMMA (M_w 950k, MicroChem, Newton, MA, USA) was prepared by spin-coating onto Silicon substrates as previously described (Falzone et al., 2012). After exposure to energetic electrons the latent patterns were developed for 1 min in methyl isobutyl ketone (MIBK, Sigma-Aldrich, Dorset UK):isopropyl alcohol (IPA, Sigma-Aldrich,) in a ratio of 2:1 (Falzone et al., 2012, Royle et al., 2015).

Electron beam calibration of resist response

The dose calibrations were obtained using an electron beam lithography system (JEOL JBX 5500FS, Peabody, MA, USA) operated under high vacuum at an accelerating voltage of 25

keV with a beam current of 13 nA. To avoid unnecessary pixelation due to the larger step sizes the electron beam was slightly defocused. The resists were exposed to a range of electron fluences (i.e. $1 \times 10^5 \text{ e}^-/\mu\text{m}^2$ - $1 \times 10^8 \text{ e}^-/\mu\text{m}^2$) (Falzone et al., 2011).

Cell culture, radiolabeling and preparation of specimens

The SQ20B cell line (American Type Culture Collection, VA, USA), derived from a laryngeal squamous cell carcinoma, was cultured in Dulbecco's modified Eagle's medium (DMEM; Sigma-Aldrich) supplemented with 10% fetal calf serum (Invitrogen, Paisley, UK) and 100 units/mL penicillin and 100 $\mu\text{g}/\text{mL}$ streptomycin (Invitrogen) in a standard humidified incubator at 37°C and 5% CO_2 . A total of 2×10^5 cells were seeded per well in a 24 well plate and left to attach overnight. Human epidermal growth factor (hEGF, Peprotech, NJ, USA) was derivatized with DTPA and labeled to a specific activity of 6-8 MBq/ μg , 40 nM DTPA-EGF, with ^{111}In acetate (Perkin Elmer, US) to produce ^{111}In -DTPA-hEGF (Reilly et al., 2000, Reilly et al., 2004). After radiolabeling, cells were incubated for 24 h at 37°C. The cell nuclei were isolated through selective lysis of the cell membrane, by exposing cells to NP-40 (0.5%) in PBS for 6 min at 4°C (Cornelissen et al., 2009). Samples were washed in d. H_2O and air dried. An inverted photoresist was placed directly on top of the cells. Cells and isolated cell nuclei treated with the radionuclide construct, were left in contact with the photoresist surface for four half-lives.

Atomic-Force Microscopy (AFM)

AFM was performed using a Park Autoprobe CP-II instrument (Veeco, UK; now Bruker, Cambridge, UK) under ambient laboratory conditions as previously described (Falzone et al., 2012, Falzone et al., 2011, Royle et al., 2015). Imaging was carried out in the intermittent contact mode using conical AFM probes (Ultrasharp NSC35/Al BS, Micromasch, Tallinn), with resonance frequencies greater than 100 kHz. The raw images were levelled with a low-

order polynomial function, and 3x3 filtering was applied in some cases to suppress electronic and acoustic noise.

Results

Experimental basis for the method

It has been shown that the local depth of a pattern in the resist is linearly dependent on the local fluence (Falzone et al., 2012, Falzone et al., 2011). The relationship between local fluence and depth of pattern in PMMA950 is shown in Figure 2. The sensitivity of the resist imposes the lower limit on the detectability of fluence. The data in Figure 2 show that depths of patterns less than approximately 2 nm, corresponding to a fluence of $1 \times 10^5 \text{ e}^-/\mu\text{m}^2$ cannot be detected reliably due to the surface roughness of the resist film. For modelling purposes, three underlying assumptions are made a) the fluence arising from internalized ^{111}In is approximated as a 25 keV mono-energetic e-beam (Supplementary material, Table 1) b) contributions to the total fluence from separate point sources are additive, and c) radiation is emitted isotropically. Thus the fluence from a point source falls off as the inverse square of the distance from the source.

[Figure 2]

Derivation of the formalism

The objective was to develop an intuitive and simple formalism for modeling the topographic features of patterns in the developed resist following exposure from a radionuclide treated cell or cell nucleus. The simplicity is derived from the placement of one or more point sources, each emitting a total number of electrons, F_{0i} , at a distance Z_i above a location in the x-y plane of the resist (Figure 3). The parameters F_{0i} and Z_i and the x-y locations can be adjusted for a best fit to the topography of the pattern.

[Figure 3]

The fluence a distance R from a point source is:

$$F_{iR} = \frac{F_{0i}}{4\pi R^2} \quad \text{in } e^-/\mu\text{m}^2 \quad (1)$$

The two unknowns, Z_i and F_{0i} ; can be determined from two experimental observables; (1) the radius of the pattern, r_i , bounded by the minimum detectable local fluence, $1 \times 10^5 \text{ } e^-/\mu\text{m}^2$ (Falzone et al., 2011, Royle et al., 2015), and (2) the greatest depth of the pattern, D_i , corresponding to the maximum local fluence at the original surface of the resist. At the boundary of the pattern the fluence is:

$$1 \times 10^5 = \frac{F_{0i}}{4\pi(Z_i^2 + r_i^2)} \quad (2)$$

At the deepest part of the pattern we have:

$$F_i(r'_i = 0) = \frac{F_{0i}}{4\pi Z_i^2} \quad (3)$$

From the calibration data in Figure 2 we see that the local fluence, $F_i(r'_i)$, is linearly dependent on the local depth of the pattern; therefore it is convenient to replace $F_i(r'_i)$ at an arbitrary point along a contour line defining the pattern by $10^{-5}C_i(r'_i)$, where $C_i(r'_i)$ can range from 1 to 1250 (Falzone et al., 2011). Therefore Eq. (3) can be rewritten as:

$$F_{0i} = 4\pi \times 10^5 C_i(r'_i) Z_i^2, \quad \text{for } r'_i = 0 \quad (4)$$

Thus Eq. (2) can be rewritten as:

$$C_i(r'_i) Z_i^2 = (Z_i^2 + r_i'^2) \quad (5)$$

Solving for Z_i at the deepest point of the pattern:

$$Z_i = \sqrt{\frac{r_i'^2}{C_i(r'_i=0)-1}} \quad (6)$$

Eqs. (4) and (6) can now be used to determine numerical values for Z_i and F_{0i} (the locations of point sources in the z -direction and the total fluence of the respective sources). The depth of the pattern along a contour line at locations defined by $r_i > r'_i > 0$ can then be determined from the following expression:

$$C_i(r'_i) = \frac{c_i(r'_i=0)Z_i^2}{Z_i^2 + r_i'^2} \quad (7)$$

A nomogram of Eq. 7 is shown in Figure 4. The height of a point source is plotted as a function of greatest depth of the pattern with the radius of the pattern as a parameter. The maximum height of 1 μm was informed by AFM analysis of a fixed cell (Supplementary Figure 1). The family of curves allows a more rapid approximate modeling of any pattern without recourse to the detailed formalism. It is particularly useful when multiple point sources are required in order to obtain a reasonably good fit.

Having identified the height of the point source above the resist plane, the total number of electrons emitted by the point source can be determined by

$$F_{0i} = 4\pi \times 10^5 C_i(r'_i = 0) Z_i^2 \text{ (electrons)} \quad (8)$$

[Figure 4]

The shape of the pattern resulting from the placement of a point source above a plane resist surface was calculated from the formalism, and is shown as a dotted grey line in Figure 5. It can be seen from the formalism that the shape defined by two concave lines remains the same for all point sources, regardless of location and activity. The merits of the procedure described in the previous section will now be explored for several actual patterns, beginning with a simple example in Figure 5, and progressing to more detailed patterns. In the case of the pattern shown in Figure 5 the estimated value of Z_1 of 500 nm was obtained from the nomogram, while the total number of electrons emitted by the point source, $F_{01} = 8.0 \times 10^6$, was calculated from Eq. 8.

[Figure 5]

More complex patterns of cell nuclei after 24 h exposure to the ^{111}In -labeled construct are demonstrated in Figure 6. To arrive at a better fit in this case, more than one point source was

used. Contour lines were used to identify the optimal locations in the x-y plane for placement of the sources, these were placed above the different positions of maximum depth.

[Figure 6]

[Table I]

Discussion

An important aspect when evaluating an Auger electron-emitting radionuclide for therapeutic purposes is the intracellular and cell nucleus spatial distribution of the construct. Due to the short range of Auger electrons it is imperative that the Auger emitter is closely associated with the DNA to maximise its biological cell killing potential (Kassis, 2004). However, herein lies the problem, current methods used to assess spatial distribution of TRT agents such as MAR are not able to provide quantitative information about the spatial distribution of AEs at a resolution similar to their range in biological material. MAR can distinguish between the number of grains in the cell nucleus and cytoplasm, but is limited by the physical size of the silver grains, non-uniform emulsion coverage of the sample and the diffraction limit of optical microscopy (Puncher and Blower, 1994). On the other hand, with PAR the whole resist surface is a continuous sensitive detector of electron fluence and the AFM readout of the chemically etched patterns can provide a lateral resolution of a few nm. The challenge with both techniques however remain to predict the possible positions of the radionuclides in a 3-D space responsible for the respective patterns.

In this report, we present a simple mathematical model based on the radius and depth of radiation-induced patterns in photoresist material to identify the location in the z-plane of an ¹¹¹In source capable of generating the pattern. By using fluence vs. pattern-depth calibration data, generated by e-beam lithography (Figure 2), a nomogram (Figure 4) is presented that relates the experimental observables, (radius and pattern depth) to the z-position. This model is a novel approach and has not previously been presented and was necessitated as the e-beam

could not be used to investigate the effect of sources at different distances above the surface of the resist (and so simulate ^{111}In at different positions in the z-plane in cells). This is because lithographic instruments used for generating e-beam patterns, such as the one used for the experiments reported here, operate under high vacuum, enabling fluence to be controlled with precision. Thus, the e-beam fluence is constant under vacuum regardless of the position of the e-beam source.

With the experimental system used for illustrative purposes in this manuscript, i.e. head and neck cancer cells treated with ^{111}In -DTPA-hEGF, it has been reported that ^{111}In -DTPA-hEGF internalizes and translocates to the cell nucleus (Bailey et al., 2007, Cai et al., 2008). Furthermore, it has been observed for this and other radiotherapeutics that there is a non-uniform distribution of radiation sources throughout all of the cellular compartments (i.e. cell membrane, cytoplasm and nucleus) (Bolch, 2008, Bousis et al., 2010, Rajon et al., 2011). The features in the resist patterns of treated cells or isolated cell nuclei are suggestive of accumulation of the internalized radionuclides at certain sites.

To test this hypothesis, we applied the mathematical formalism to simple patterns as demonstrated in Figure 5 or to more complex patterns as demonstrated in Figure 6. A good fit of the model to the shape of the pattern in Figure 5 (d), was obtained, although the fit nearer the edges of the patterns is not as robust. This may be due to the lower energy electrons near the edge of the pattern, which have a shorter residual range and inelastic mean free path (IMFP). For instance, a 20 keV electron slowing down in an organic material has a range of approximately 3 μm and an IMFP of 10 nm. For an energy of 100-200 eV the range is 10 nm and the IMFP is 1 nm (Seah and Dench, 1979). Accordingly a primary electron will enter the PMMA resist with lower energy towards the edges of a pattern, in comparison with electrons that enter the PMMA at perpendicular incidence. Although the fluence decreases towards the edges, due to the $1/R^2$ factor, those which impact the resist with a lower energy, have a shorter

IMFP, and will therefore be more efficient at producing chain scissions per unit path length in the PMMA. Another contributing factor is that small-angle scattering will make a marginal contribution towards the broadening of a pattern. This is due to a very slight excess fluence near the boundary of a pattern, mainly as a consequence of the additional path length being the cause of additional scattering.

An important aspect to take into consideration when using an AFM to image nanoscale surface features, is that the resolution of the image may be limited by the shape of the tip of the AFM probe in relation to the shape of the feature itself. A routine probe tip has a radius of curvature at the apex of about 10 nm, although this can vary up to 50 nm. The feature can interact with the sides of the probe, leading to an image which is a combination of the actual topography of the feature and the probe geometry (Dufrène, 2002). Likewise, the shaft of the tip has an opening half-angle of 20° , which places a limit on the steepness of slope that can be tracked by the tip apex (Supplementary Figure 2). Variations from this angle will cause artefacts in the imaging of the photoresist surface (Calabri et al., 2008).

A potential caveat that has to be taken into account when evaluating the PAR technique, is the assumption that the emissions from ^{111}In can be approximated by a monoenergetic 25 keV electron beam on which the calibration of the resist response was based. ^{111}In emits electrons with energies ranging from a few eV (Auger and Coster-Kronig electrons up to 26 keV) to a few hundreds of keV (internal conversion electrons up to 250 keV). Ideally, the response of the photoresist should be calibrated using an electron beam or beams with energies identical to those of the electrons emitted by the radionuclide of interest. The limitation of calibration energy used herein was set by the electron beam lithography system which could only operate at beam energies of 50 and 25 keV. Regardless, for the development conditions used in this study, PMMA950 is relatively insensitive to a variation in electron energy (Falzone et al., 2012). Furthermore, the choice of a 25 keV electron beam to calibrate the photoresists was

informed by both the yield and energies of electrons emitted by ^{111}In which gave an average weighted electron energy of 35 keV (Royle et al., 2015). From supplementary data (Table 1) we show that there is at most a three-fold difference in fluence between the emissions from ^{111}In and the 25 keV e-beam calibration data depending on the source position. Nonetheless, the 25 keV e-beam provides an adequate approximation for electron emissions from ^{111}In . Indeed, the straightforward modeling approach based on the 25 keV e-beam calibration method described in the current report, provides a good match for the experimental data (Figure 5d).

Additionally, we previously reported that patterns arising from e-beam fluences as low as $6.2 \times 10^4 \text{ e}^-/\mu\text{m}^2$ ($1 \mu\text{C}/\text{cm}^2$) were readily detectable by AFM analysis (Falzone et al., 2011, Royle et al., 2015). However surface roughness after chemical development could potentially limit the interpretation of such patterns, therefore a threshold for detection was set to $1 \times 10^5 \text{ e}^-/\mu\text{m}^2$. By assuming a threshold of detection we are potentially introducing an error in fluence estimation. Thus, taken together with the uncertainty in the use of 25 keV monoenergetic calibration data, more development of the technique is required to relate the depth of etched patterns to potential source positions.

In this regard, Monte Carlo simulation of source positions informed by the variation in fluence observed in patterns from treated cells could provide a more accurate estimation of z-position. The technique outlined in this paper could therefore be used as a starting point for z-position simulation of more complex patterns. The greatest challenge would be to provide more accurate calibration data for ^{111}In as the use of microspheres cannot fully simulate the distribution of ^{111}In in a 3-D cell. A future direction of this research could investigate the use of cellular dimension structures integrated with known amounts of radioactivity. Additionally, co-registration of a microscopic image of a cell with the photoresist pattern to which it gave

rise would allow more accurate spatial mapping of the pattern or particular features within the pattern to subcellular structures such as the nucleus.

Conclusions

An intuitive and simple procedure has been developed for identifying the locations and fluence resulting from Auger electron-emitting radionuclides internalized within cancer cells. The procedure consists of matching an experimental 3-D pattern in a photoresist film detector by placement of one, or more, point sources at locations, with known fluence that can be inferred from two experimental parameters (the local depth of the pattern and its radius in the x-y plane). This methodology could be extended in future to provide the input for Monte Carlo simulation of complex PAR patterns.

Acknowledgements With special thanks to Dr. Alison Crossley and Dr. Colin Johnston at the Oxford University Begbroke Science Park, and the Department of Physics for the use of facilities.

Declaration of interest

The authors report no conflict of interest. The authors alone are responsible for the content and writing of the paper.

This work is supported by Cancer Research UK (C5255/A15935), the Medical Research Council and the CR-UK Oxford Cancer Imaging Centre.

References

- BAILEY, K. E., COSTANTINI, D. L., CAI, Z., SCOLLARD, D. A., CHEN, Z., REILLY, R. M. & VALLIS, K. A. 2007. Epidermal growth factor receptor inhibition modulates the nuclear localization and cytotoxicity of the Auger electron emitting radiopharmaceutical ^{111}In -DTPA human epidermal growth factor. *J Nucl Med*, 48, 1562-70.
- BOLCH, W. 2008. Further explorations of cellular uptake of radioactivity. *J Nucl Med*, 49, 869-870.
- BOUSIS, C., EMFIETZOGLOU, D., HADJIDOUKAS, P. & NIKJOO, H. 2010. Monte Carlo single-cell dosimetry of Auger-electron emitting radionuclides. *Phys Med Biol*, 55, 2555-72.
- CAI, Z., CHEN, Z., BAILEY, K. E., SCOLLARD, D. A., REILLY, R. M. & VALLIS, K. A. 2008. Relationship between induction of phosphorylated H2AX and survival in breast cancer cells exposed to ^{111}In -DTPA-hEGF. *J Nucl Med*, 49, 1353-61.
- CALABRI, L., PUGNO, N., MENOZZI, C. & VALERI, S. 2008. AFM nanoindentation: tip shape and tip radius of curvature effect on the hardness measurement. *J Phys Condens Matter*, 20, 474208.
- CORNELISSEN, B., KERSEMANS, V., MCLARTY, K., TRAN, L. & REILLY, R. M. 2009. ^{111}In -labeled immunoconjugates (ICs) bispecific for the epidermal growth factor receptor (EGFR) and cyclin-dependent kinase inhibitor, p27Kip1. *Cancer Biother Radiopharm*, 24, 163-73.
- DUFRENE, Y. F. 2002. Atomic Force Microscopy, a Powerful Tool in Microbiology. *J Bacteriol*, 184, 5205-5213.
- FALZONE, N., MYHRA, S., CHAKALOVA, R., ROYLE, G., ALTEBAEUMER, T., NATHAN, R. & VALLIS, K. A. 2012. Photoresists as a high spatial resolution

- autoradiography substrate for quantitative mapping of intra- and sub-cellular distribution of Auger electron emitting radionuclides. *Int J Radiat Biol*, 88, 933-40.
- FALZONE, N., NATHAN, R., MYHRA, S., CHAKALOVA, R., ALTEBAEUMER, T. & VALLIS, K. 2011. Chemically amplified photoresist for high resolution autoradiography in targeted radiotherapy. *Biomaterials*, 32, 6138-44.
- HOWELL, R. W., RAJON, D. & BOLCH, W. E. 2012. Monte Carlo simulation of irradiation and killing in three-dimensional cell populations with lognormal cellular uptake of radioactivity. *Int J Radiat Biol*, 88, 115-22.
- JACKSON, M. R., FALZONE, N. & VALLIS, K. A. 2013. Advances in anticancer radiopharmaceuticals. *Clin Oncol (R Coll Radiol)*, 25, 604-9.
- KASSIS, A. I. 2004. The amazing world of auger electrons. *Int J Radiat Biol*, 80, 789-803.
- MALARODA, A., FLUX, G. & OTT, R. 2005. The application of dose-rate volume histograms and survival fractions to multicellular dosimetry. *Cancer Biother Radiopharm*, 20, 58-65.
- PUNCHER, M. R. & BLOWER, P. J. 1994. Radionuclide targeting and dosimetry at the microscopic level: the role of microautoradiography. *Eur J Nucl Med*, 21, 1347-65.
- RAJON, D., BOLCH, W. E. & HOWELL, R. W. 2011. Lognormal Distribution of Cellular Uptake of Radioactivity: Monte Carlo Simulation of Irradiation and Cell Killing in 3-Dimensional Populations in Carbon Scaffolds. *J Nucl Med*, 52, 926-933.
- REILLY, R. M., KIARASH, R., CAMERON, R. G., PORLIER, N., SANDHU, J., HILL, R. P., VALLIS, K., HENDLER, A. & GARIEPY, J. 2000. ¹¹¹In-labeled EGF is selectively radiotoxic to human breast cancer cells overexpressing EGFR. *J Nucl Med*, 41, 429-38.
- REILLY, R. M., SCOLLARD, D. A., WANG, J., MONDAL, H., CHEN, P., HENDERSON, L. A., BOWEN, B. M. & VALLIS, K. A. 2004. A kit formulated under good

manufacturing practices for labeling human epidermal growth factor with ^{111}In for radiotherapeutic applications. *J Nucl Med*, 45, 701-8.

ROYLE, G., MYHRA, S., CHAKALOVA, R., VALLIS, K. A. & FALZONE, N. 2015.

Spatial distribution of Auger electrons emitted from internalised radionuclides in cancer cells: the photoresist autoradiography (PAR) method. *Radiat Prot Dosimetry*, 1-5.

SEAH, M. P. & DENCH, W. A. 1979. Quantitative electron spectroscopy of surfaces: A standard data base for electron inelastic mean free paths in solids. *Surf Interface Anal*, 1, 2-11.

Tables

Table I.

A summary of the experimental and modelling information obtained from Figure 6; R_x is the radius of the pattern and D_x is the depth of a pattern at the x-y location of the point source. The following parameters are obtained from modeling; the local fluence, C_x (10^5), the height that the source is located above the surface of the resist, Z_x and the total number of electrons emitted from the point source, F_{0x} .

	Pattern (a)		Pattern (b)		Pattern (c)		
	L_1	L_2	L_1	L_2	L_1	L_2	L_3
Radius (R_x , μm)	0.6	0.5	0.6	1.1	2.4	2.1	1.4
Depth (D_x , nm)	50	74	36	95	68	66	75
Fluence (C_x , $\text{e}^-/\mu\text{m}^2$)	10	15	7.0	19	14	13	15
Height (Z_x , nm)	200	130	240	260	600	420	360
Electrons emitted (F_x , e^-)	5.03×10^5	3.19×10^5	5.07×10^5	1.61×10^5	6.33×10^5	2.88×10^5	2.44×10^5

Figures

(a) Treatment of cells with radiolabeled construct



(b) Exposure



(c) Development



(d) Analysis

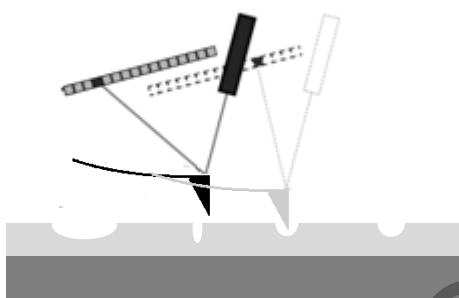


Figure 1. Schematic representation of the experimental sequence. (a) Cells are incubated with an Auger electron-emitting radionuclide. (b) Exposure of a PMMA photoresist film in close proximity to the cells/nuclei. (c) Chemical development of the latent images. (d) Topographic imaging by AFM to reveal the 3-D structure of the pattern.

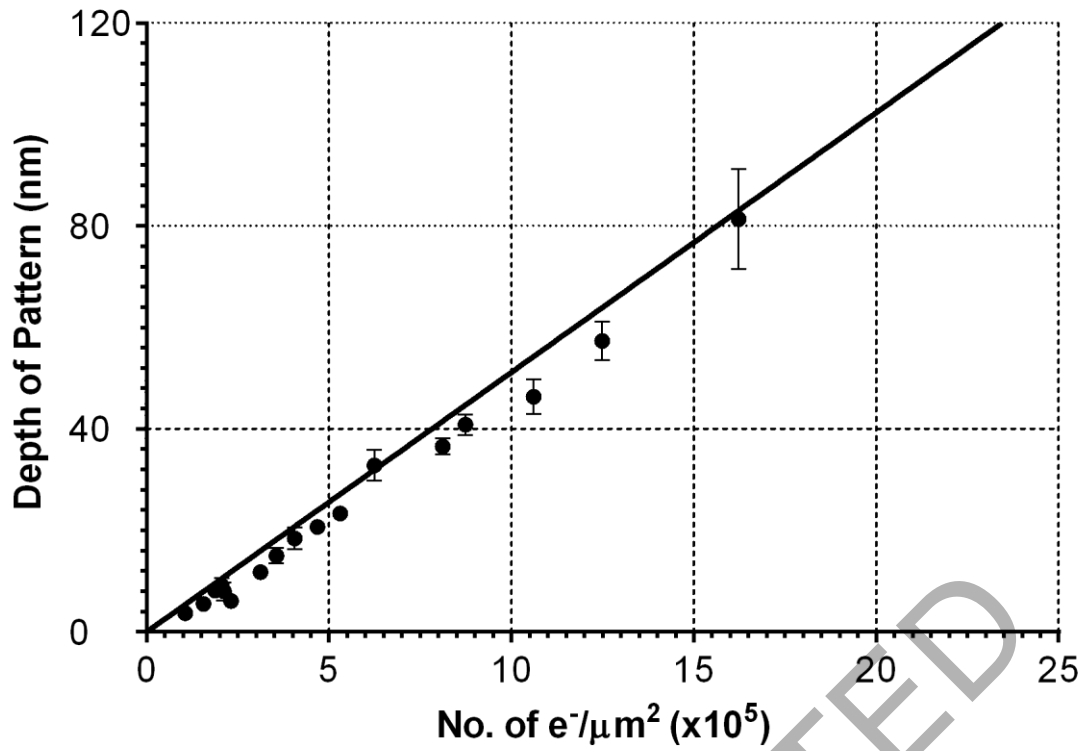


Figure 2. The sensitivity of PMMA950 photoresist to irradiation by 25 keV electrons for development times of 60 s. The depth of the developed pattern is linearly dependent on the fluence. The limit of detectability (z resolution) was 2-3 nm, corresponding to a fluence of approximately $1 \times 10^5 \text{ e}^-/\mu\text{m}^2$, and was defined as the depth at which the features of a $5 \times 5 \mu\text{m}^2$ pattern in the AFM image was unresolvable due surface roughness (Falzone et al., 2012, Falzone et al., 2011).

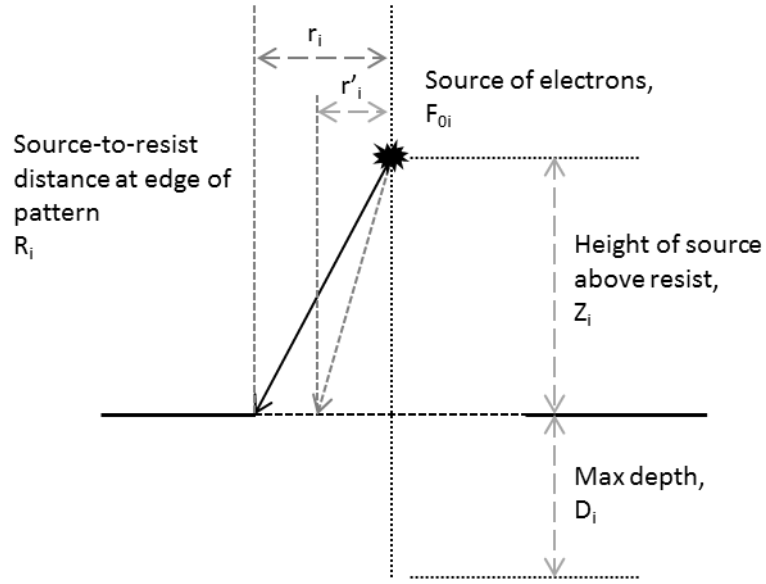


Figure 3. The schematic shows a point source delivering a total number of electrons, F_{0i} , into the 4π solid angle from a location a distance Z_i above the plane of the resist. The radius of the resultant pattern in the x-y plane, r_i , is defined by the resist having received a fluence greater than $1 \times 10^5 \text{ e}^-/\mu\text{m}^2$ (from calibration data). The greatest depth of the pattern, D_i , is measured from the original height of the resist surface. The local depth of the pattern is linearly related to the local fluence incident on the original resist surface.

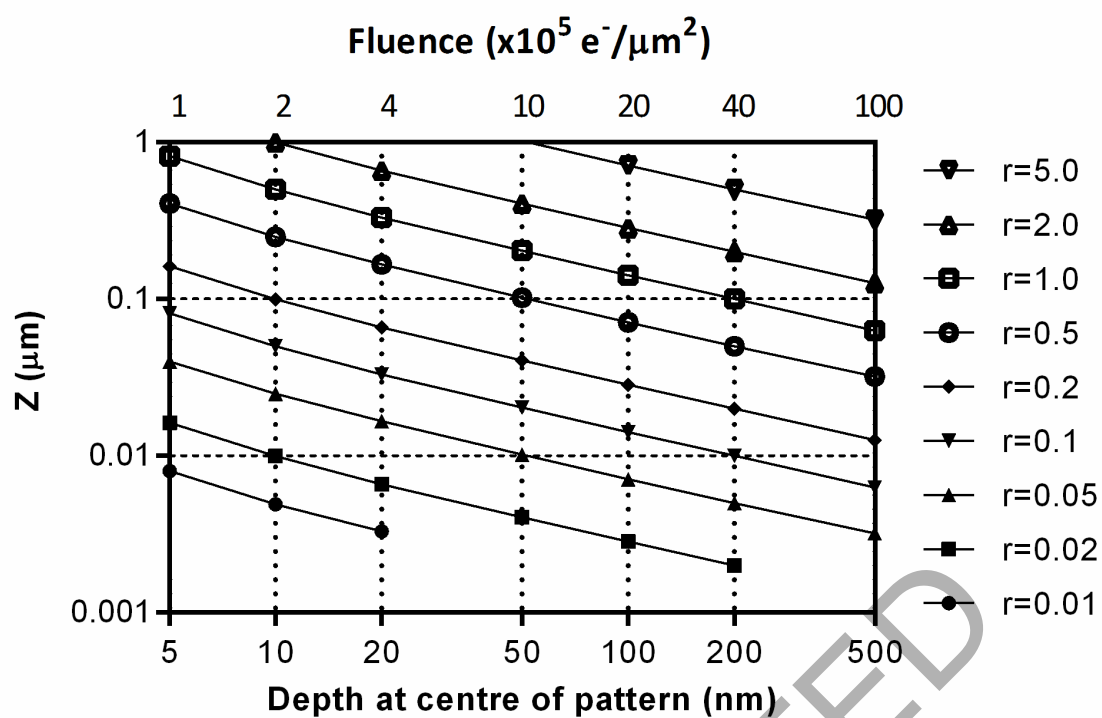


Figure 4. Nomogram showing the relationship between experimental observables, (depth at centre of pattern, in nm, and radius of pattern, in μm), and location of a point source above the plane of the resist. Interpolation between the curves allows for quick interpretation of features in an image.

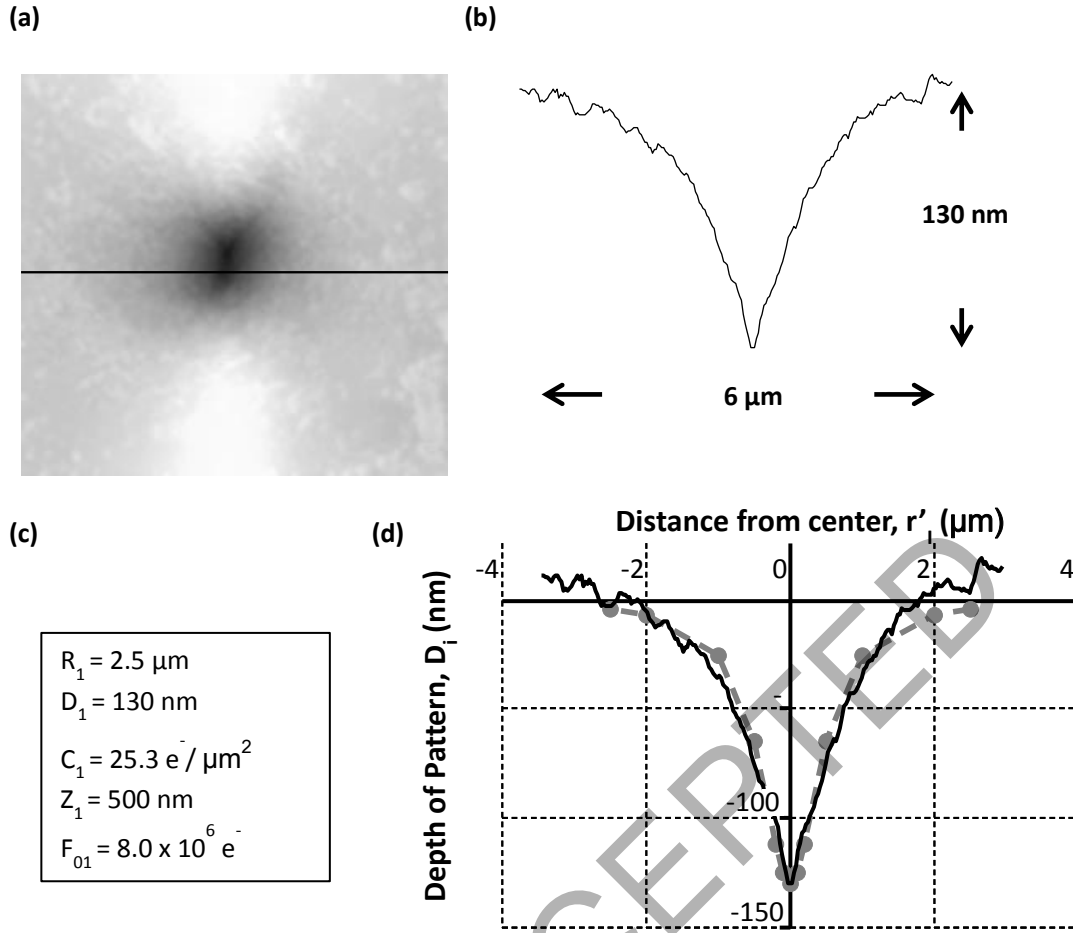


Figure 5. (a) AFM image of a pattern from a cell nucleus with internalized ^{111}In . The AFM-derived contour line through the centre of the pattern is shown in (b). The measured depth and radius were 130 nm and 2.5 μm , respectively. Using equations (6) and (10), the information shown in the table (c) can be obtained. (d) Demonstrates the goodness of fit from placement of a single point source emitting 8.0×10^6 electrons (F_{0i}), at a height 500 nm above the resist (Z_i). Good agreement between the experimental data (solid black line) and model is shown by the shape of a theoretical contour line (grey broken line) as modeled from Eq. 7.

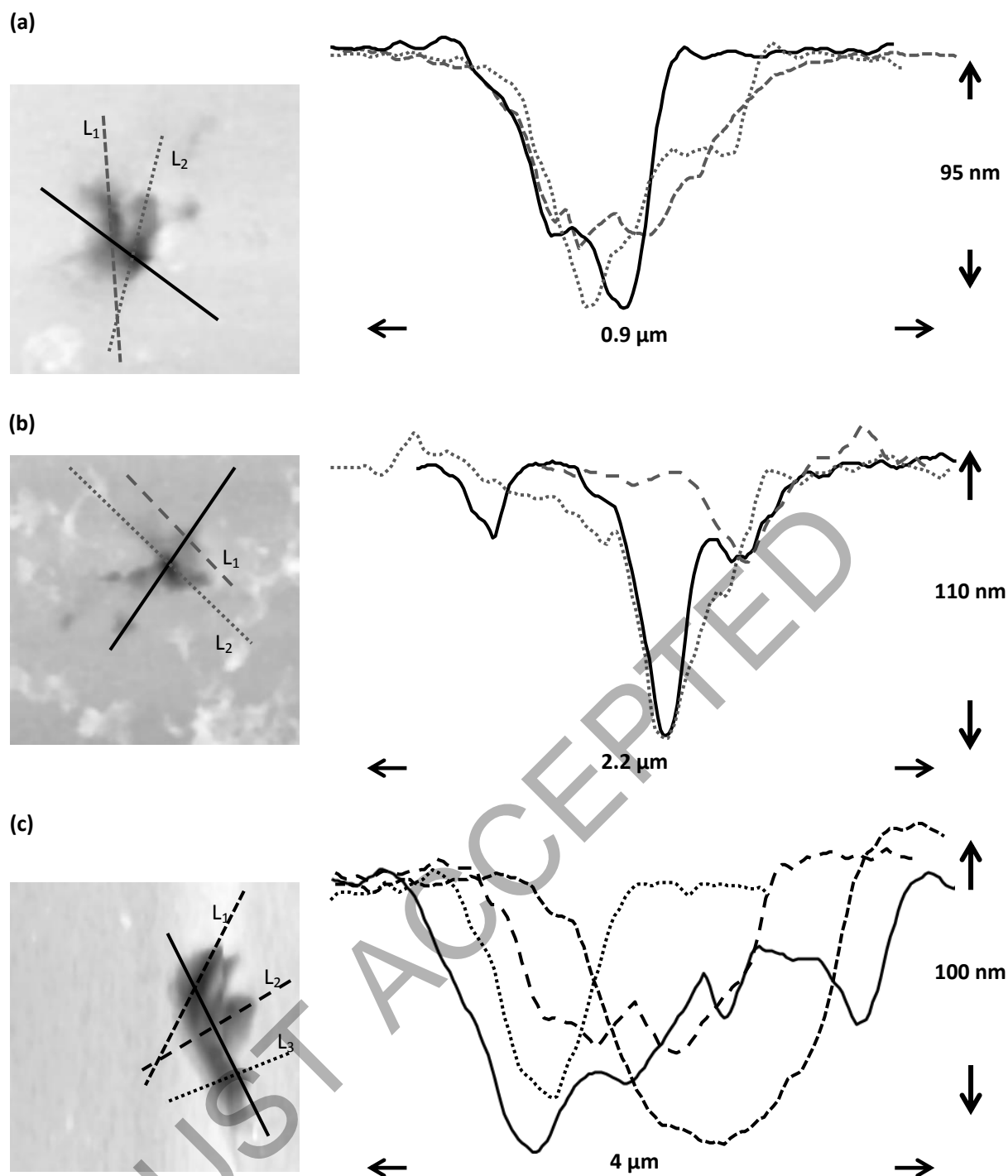


Figure 6. A demonstration of modeling of increasingly complex patterns from isolated cell nuclei, incubated with ^{111}In -DTPA-EGF for 24 h. The actual patterns are shown, with line scans ($L_{1,2,3}$) representing the regions of greatest depth. A summary of the experimental and modeling information is provided in Table I.